Microsecond Folding of the Cold Shock Protein Measured by a Pressure-Jump Technique†

Maik Jacob,‡ Georg Holtermann,§ Dieter Perl,‡ Jochen Reinstein,§ Thomas Schindler,‡ Michael A. Geeves,*,§,|| and Franz X. Schmid*,‡

Biochemisches Laboratorium, Universität Bayreuth, D-95440 Bayreuth, Germany, and Max-Planck-Institut für molekulare Physiologie, Rheinlanddamm 201, D-44139 Dortmund, Germany

Received October 19, 1998; Revised Manuscript Received December 30, 1998

ABSTRACT: A pressure-jump apparatus was employed in investigating the kinetics of protein unfolding and refolding. In the reaction cell, the pressure can be increased or decreased by 100−160 bar within 50−100 μs and then held constant. Thus, unfolding and refolding reactions in the time range from 70 μs to 70 s can be followed with this technique. Measurements are possible in the transition regions of thermally or denaturant-induced folding in a wide range of temperatures and solvent conditions. We used this pressure-jump method to determine the temperature dependence of the rate constants of unfolding and refolding of the cold shock protein of *Bacillus subtilis* and of three variants thereof with Phe → Ala substitutions in the central β-sheet region. For all variants, the change in heat capacity occurred in refolding between the unfolded and activated states, suggesting that the overall native-like character of the activated state of folding was not changed by the deletion of individual Phe side chains. The Phe27Ala mutation affected the rate of unfolding only; the Phe15Ala and Phe17Ala mutations changed the kinetics of both unfolding and refolding. Although the activated state of folding of the cold shock protein is overall native-like, individual side chains are still in a non-native environment.

The rates of protein folding reactions cover many orders of magnitude. Large proteins often require minutes or even hours for folding (*1*, *2*), whereas some small proteins can complete their folding within a few milliseconds or even faster (*3*−*13*). Domains of large proteins presumably also fold rapidly, but the assembly of prefolded domains can be slow and thus rate-limiting for overall folding. The discovery of the fast-folding proteins and new theoretical concepts, such as the use of complex energy landscapes to model protein folding reactions (*14*, *15*), has revived the interest in methods for following very rapid folding processes. The situation is thus similar to the one 30 years ago when the application of stopped-flow and temperature-jump methods revealed that proteins such as lysozyme, ribonuclease A, or cytochrome *c* can complete folding within ≤1 s (*16*−*19*).

The dead time of conventional stopped-flow spectroscopy is 1−2 ms; faster processes cannot be investigated using this technique. Recently, several methods have been applied to break this millisecond barrier (*20*). They include ultrafast turbulent mixing techniques (*8*−*10*), the photochemical triggering of a folding reaction (*21*−*23*), NMR relaxation methods (*4*, *12*), and laser-induced temperature jumps (*24*−*27*).

The equilibrium unfolding of a protein is often accompanied by a decrease in reaction volume (*28*−*33*), and therefore, unfolding can be induced by a sudden increase and refolding by a sudden decrease in pressure. Such pressure jumps are very gentle. They do not involve significant heating (≤0.0015 °C/bar), mechanical mixing, or intense irradiation, and cycles of combined up and down pressure jumps can be used to determine the kinetics of both unfolding and refolding with a single sample.

In previous experiments, Pryse et al. (*34*) investigated the folding kinetics of cytochrome *c* after small 15 bar pressure jumps. The folding equilibrium was displaced to a minor extent only in these experiments, and therefore, a very high protein concentration and a large time constant were necessary to increase the signal/noise ratio. In the experiments described here, the pressure could be changed by 160 bar within less than 100 μs. Therefore, much larger amplitudes were observed, and the time resolution allowed measurements in the microsecond range. We used this pressure-jump technique to extend our previous stopped-flow measurements of the fast folding of the cold shock proteins from *Bacillus subtilis* (*Bs*-CspB)[1] and *Bacillus caldolyticus* (*Bc*-Csp). Folding could be followed at protein concentrations of 20 μg/mL in the time range between 50 μs and 70 s and at temperatures as high as 80 °C. The good performance of the pressure-jump apparatus over a wide range of tempera-

† This work was supported by grants from the Deutsche Forschungsgemeinschaft and the Fonds der Chemischen Industrie.

* Corresponding authors. E-mail: geeves@ukc.ac.uk or FX.Schmid@uni-bayreuth.de.

‡ Universität Bayreuth.

§ Max-Planck-Institut für molekulare Physiologie.

|| Present address: Department of Biosciences, University of Kent, Canterbury, Kent CT2 7NJ, U.K.

[1] Abbreviations: *Bs*-CspB, cold shock protein B from *B. subtilis*; *Bc*-Csp, cold shock protein from *B. caldolyticus*; N and U, native and unfolded forms of a protein, respectively; TS, transition state; Θ, ellipticity; λ, measured (apparent) rate constant; k_{ij}, microscopic rate constant; GdmCl, guanidinium chloride.

10.1021/bi982487i CCC: $18.00
Published on Web 02/13/1999

tures allowed us to determine the activation enthalpies, entropies, and heat capacities of unfolding and refolding of *Bs*-CspB and to characterize the effects of several Phe → Ala substitutions on the folding mechanism.

MATERIALS AND METHODS

Materials. CspB from *B. subtilis* was overexpressed in *Escherichia coli* using the bacteriophage T7 RNA polymerase promotor system (*35*) and purified as described previously (*6*). The construction and purification of the variants with single Phe → Ala replacements at positions 15, 17, and 27 have been described (*36*, *37*). Csp from *B. caldolyticus* was purified according to ref *36*.

Heat-Induced Equilibrium Unfolding Transitions. Thermal denaturation and renaturation curves were followed by the change in ellipticity at 223 nm, which decreased from about 2000 deg cm^2 dmol^{-1} at 10 °C to about −3000 deg cm^2 dmol^{-1} at 70 °C for wild-type *Bc*-CspB. Similar but not identical CD changes were observed for the three Phe → Ala variants. CD was measured with a Jasco J 600 spectropolarimeter equipped with a Peltier element. The temperature in the cuvette was measured with a thermosensor. Its accuracy was checked by using a calibrated precision thermometer (Brand, Wertheim, Germany). The protein concentrations were 3−16 μM in 1 cm cells, and the buffer was 0.1 M sodium cacodylate/HCl (pH 7.0). The samples were heated at a rate of 1.5 °C/min. The reversibility was examined by subsequently cooling the samples to the starting temperature. The midpoints of the heating and cooling curves differed by <1 °C, and the original ellipticity was regained after the heating/cooling cycles. The unfolding transition curves were analyzed by a nonlinear least-squares fit of Θ_{223} as a function of temperature to eq 1 (*37*) using the programs Grafit 3.0 (Erithacus Software, Staines, U.K.) and Scientist (Micromath, Salt Lake City, UT). Equation 1 relates the dependence on temperature of the ellipticity to the thermodynamics of a two-state unfolding reaction.

$$\Theta(T) = \Theta_N - \frac{\Theta_N - \Theta_U}{1 + \exp[\Delta G(T)/RT]} \tag{1a}$$

with

$$\Theta_N = \Theta_N^\circ + m_N T \tag{1b}$$

$$\Theta_U = \Theta_U^\circ + m_U T \tag{1c}$$

and

$$\Delta G(T) = \Delta H_M - T\Delta S_M + \Delta C_p\left[(T - T_M) - T\,1n\left(\frac{T}{T_M}\right)\right] \tag{2}$$

In eq 2, ΔH_M, ΔS_M, and ΔC_p are the enthalpy, entropy, and heat capacity of protein unfolding at T_M, the temperature where 50% of the protein molecules are in an unfolded state. The ellipticity of the native protein (Θ_N) and the unfolded protein (Θ_U) are assumed to depend linearly on temperature. The values of Θ_N° and Θ_U° are those at 0 K, and m_N and m_U define the dependencies of Θ_N and Θ_U on temperature, respectively. The equilibrium constant of unfolding, K, is calculated by using eq 3.

$$K(T) = \exp\left[-\frac{\Delta G(T)}{RT}\right] \tag{3}$$

The three Phe → Ala variants are less stable than wild-type CspB, and the baselines of the folded proteins are not reached at low temperatures before the onset of cold denaturation. For these variants, the baselines for the native proteins were measured in the presence of 36% ethylene glycol. This additive stabilizes CspB (*38*) but does not affect the ellipticity at 223 nm of native CspB and its dependence on temperature. The GdmCl-induced equilibrium transitions were analyzed by assuming a linear two-state mechanism and by using the procedure of Santoro and Bolen (*39*).

Pressure-Jump Apparatus. A pressure-jump apparatus was built using an original design of Clegg and Maxfield (*40*) in which the pressure is applied to a protein solution by a stack of piezoelectric crystals (Figure 1). The sample is held in a sapphire ring which allows optical monitoring of the sample in the near-UV and visible light regions. The sample is separated from the crystal stack by a thin kaptan membrane. Two different crystal stacks are used to generate pressures (Physik Instrumente, PI-245.30 and PI-245.70). Application of up to 1000 V to the crystal stack results in an expansion of the length of the stack of up to 40 μm (PI-245.30) or 120 μm (PI-245.70) and allows forces of up to 2 kN to be applied to the membrane. With a total sample volume of 50 μL, application of 0−1000 V to the membrane results in pressures of 1−100 bar (PI-245.30) or 1−200 bar (PI-245.70). For the larger stack, the pressure change is 90% complete in 100 μs and 90% complete in about 50 μs for the smaller crystal stack. The stacks can easily be exchanged in about 15 min. Once established, the elevated pressure was stable and in the individual experiments was kept constant for times between 5 ms and 70 s before the pressure was reduced to the lower initial pressure. Pressure up and down jumps showed similar time courses. The transient response of the protein solution was recorded following both the rise and fall of pressure, and automatic repetitive applications of pressure jumps under computer control allowed the signal to be averaged for several thousand pressure jumps. Full details of the apparatus will be published separately (G. Holtermann and M. Geeves, manuscript in preparation).

In the experiments described here, the folding reactions of the cold shock proteins were followed by monitoring the changes in intrinsic tryptophan fluorescence. The fluorescence was excited at 295 nm by light from a HgXe lamp after passage of the light through a monochromator. Emission was detected at 90° relative to the incident light through a WG 345 filter. In all experiments, the final fluorescence signal was adjusted to a photomultiplier output of 10 V.

Analysis of the Folding Kinetics. For a two-state folding reaction as described in eq 4a, the measured rate constant λ is equal to the sum of the microscopic rate constants for refolding (k_{UN}) and unfolding (k_{NU}) (eq 4b). Equations 4b and 4c are used to calculate the microscopic rate constants from λ and from the equilibrium constant K (eq 3) at the respective temperature.

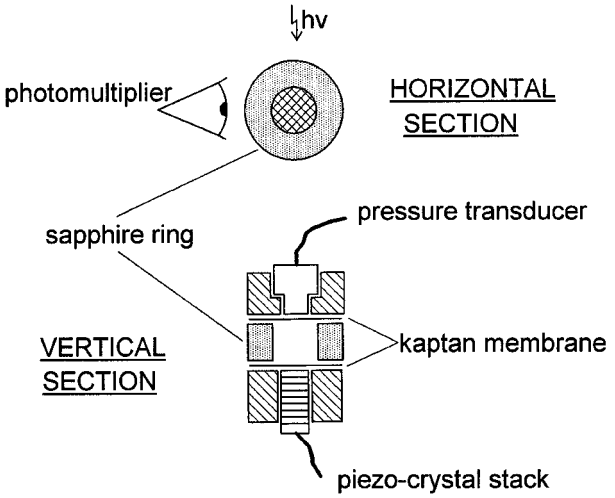

FIGURE 1: Schematic diagram of the pressure-jump apparatus. The sample (50 μL) is held in an optical chamber consisting of a sapphire ring (an inside diameter of 2 mm and an outside diameter of 5 mm with a height of 5 mm). The ends of the chamber are closed by a pressure sensor (Kistler 601A) at one end and a piston attached to a piezoelectic translator (Physik Instrumente P-245.70 or P245.30) at the other. The sample is exchanged via two valves (not shown). Fluorescence is excited by monochromatic light from a light guide, and emission is collected onto a photomultiplier at 90° to the incident light through an appropriate filter.

$$\mathrm{N} \underset{k_{\mathrm{UN}}}{\overset{k_{\mathrm{NU}}}{\rightleftharpoons}} \mathrm{U} \tag{4a}$$

$$\lambda = k_{\mathrm{NU}} + k_{\mathrm{UN}} \tag{4b}$$

$$K = \frac{k_{\mathrm{NU}}}{k_{\mathrm{UN}}} \tag{4c}$$

Transition state theory relates an individual reaction rate constant to the Gibbs free energy of the activated state relative to that of the initial state, $\Delta G^{\ddagger}$ (eq 5).

$$k_{ij}(T) = \frac{k_{\mathrm{B}}T}{h}\exp\left[\frac{-\Delta G^{\ddagger}(T)}{RT}\right] \tag{5}$$

In eq 5, k_{B}, h, and R are the Boltzmann, Planck, and universal gas constants, respectively. In analogy to the equilibrium Gibbs free energy ΔG, the activation Gibbs free energy $\Delta G^{\ddagger}$ can be decomposed into the enthalpic and entropic components as shown in eq 6.

$$\Delta G^{\ddagger}(T) = \Delta H^{\ddagger}_{\mathrm{M}} - T\Delta S^{\ddagger}_{\mathrm{M}} + \Delta C_p^{\ddagger}\left[(T - T_{\mathrm{M}}) - T\,1\mathrm{n}\left(\frac{T}{T_{\mathrm{M}}}\right)\right] \tag{6}$$

where $\Delta H^{\ddagger}$ is the enthalpy of activation, $\Delta S^{\ddagger}$ the entropy of activation, and $\Delta C_p^{\ddagger}$ the heat capacity change going from the initial to the activated state at the temperature T_{M}.

The reaction volume ΔV was calculated from the pressure dependence of the equilibrium constant K (eq 7).

$$\partial(\ln K)/\partial(P) = \Delta V/(RT) \tag{7}$$

RESULTS

Pressure-Induced Unfolding and Refolding of the Cold Shock Proteins. The cold shock proteins from *B. subtilis* (*Bs*-CspB) and from *B. caldolyticus* (*Bc*-Csp) are small proteins with 67 and 66 amino acid residues, respectively (*41*, *42*). Their tertiary structure consists of a five-stranded β-barrel; α-helices are absent (*43*, *44*). The proteins do not contain cis prolyl bonds, disulfide bonds, or tightly bound cofactors. The equilibrium transitions and the folding kinetics of both proteins are well described by a N ⇌ U two-state mechanism, where the activated state of folding is native-like in its heat capacity and in the interactions with the solvent, but lacks a fair amount of enthalpic interactions. At 25 °C and in the absence of denaturants, both cold shock proteins reach the native state with a time constant of about 1 ms, and in the middle of the unfolding transitions, unfolding and refolding are complete in about 100 ms (*6*, *7*, *36*). Thus, these folding reactions could be followed by stopped-flow methods only at low temperatures and/or in the presence of urea or GdmCl. We used *Bs*-CspB to examine whether unfolding and refolding could be induced by 160 bar pressure jumps and whether the kinetics coincide with those observed after stopped-flow mixing. The thermostable cold shock protein from *B. caldolyticus* (*Bc*-Csp) was employed to test the potential of the pressure-jump method to follow folding processes in the microsecond range at elevated temperatures.

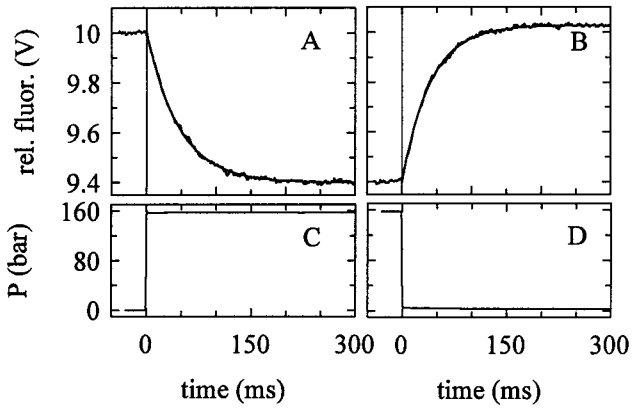

FIGURE 2: (A) Unfolding and (B) refolding of 12 μM wild-type *Bs*-CspB in 1.6 M GdmCl and 0.1 M sodium cacodylate/HCl at pH 7.0 and 25 °C following a pressure jump from 3 to 160 bar (A) and from 160 to 3 bar (B). The reaction was followed by tryptophan fluorescence. The transients were measured four times and averaged. The solid lines represent best fits to monoexponential time courses. They resulted in time constants of (A) 46 ms and (B) 40 ms. The profiles of the pressure jumps are shown in panels C and D.

Bs-CspB exhibits a low thermodynamic stability. At 25 °C, its equilibrium unfolding transition extends roughly from 0.5 to 2.5 M GdmCl with a midpoint at 1.52 M GdmCl. We used this range of GdmCl concentrations in initial experiments to examine how the U ⇌ N equilibrium of *Bs*-CspB is affected by a change in presssure. In fact, when at 1.6 M GdmCl the pressure is increased from 3 to 160 bar, the protein fluorescence decreases by about 6% (Figure 2A), which indicates that the conformational equilibrium of *Bs*-CspB is shifted toward unfolding. When, in the second half of the experiment, the pressure is relaxed from 160 to 3 bar the protein refolds and the fluorescence returns to the initial value (Figure 2B).

The pressure profiles for the unfolding and refolding experiments are shown in Figure 2C,D. The change in pressure is complete within 100 μs, and the final pressure remains stable during the measurements. Four pressure-jump cycles were performed with a total measuring time of 4 s, and the resulting averages are shown in Figure 2A,B. The

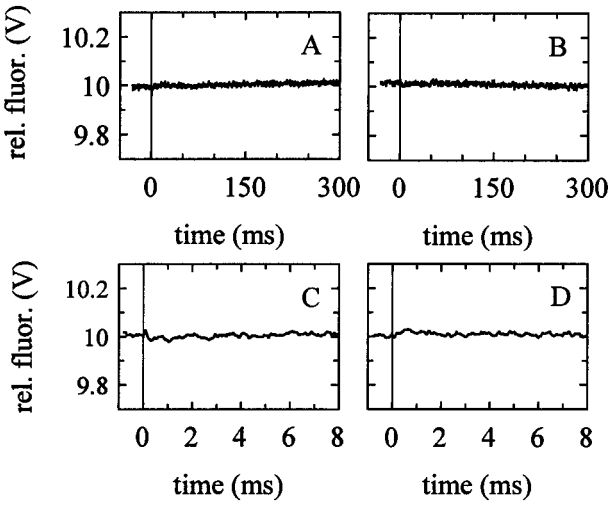

FIGURE 3: Pressure jumps at 25 °C with **(**A and B**)** unfolded wild-type *Bs*-CspB in 3.3 M GdmCl and (C and D) native wild-type *Bs*-CspB in the absence of GdmCl. Protein (12 μM) in 0.1 M sodium cacodylate/HCl at pH 7.0 was used. Jumps from 3 to 160 bar (A and C) and from 160 to 3 bar (B and D) were employed. The transients were measured 100 times and averaged.

time constant for unfolding after the 3 to 160 bar pressure jump is 46 ms (Figure 2A); for refolding after the 160 to 3 bar pressure jump, a value of 40 ms is observed (Figure 2B), in agreement with the value measured by stopped-flow spectroscopy under the same solvent conditions.

Bs-CspB unfolds when the pressure increases, which shows that the reaction volume ΔV for unfolding is negative. Upon the protein completely unfolding, the fluorescence of *Bs*-CspB is reduced by about 50% (*6*). The observed 6% decrease in fluorescence near the midpoint of the transition (Figure 2A,B) thus indicates that the 3 to 160 bar pressure jump shifts the equilibrium constant K (=[N]/[U]) from about 44/56 to about 35/65. This allows us to give a first estimate (eq 7) of ΔV of -60 ± 20 mL/mol for the unfolding of *Bs*-CspB under the given conditions. The pressure range of 160 bar that is accessible in our experiments is too small to give a more accurate ΔV value.

Pressure-induced cycles of unfolding and refolding between 160 and 3 bar as shown in Figure 2 were performed in all experiments, but only the λ values obtained at the low pressure in the refolding direction (after the 160 to 3 bar jumps) are reported for the subsequent experiments. Generally, the measured λ values were slightly smaller at 160 bar than at 3 bar, which indicates that the activation volumes of both unfolding and refolding are positive, but small. Again, the accessible pressure range of 160 bar was not wide enough to calculate explicit values for the activation volumes in either direction. Since the pressure dependence is so small, the folding rates obtained after pressure release at 3 bar are virtually identical with those obtained at atmospheric pressure.

Below 0.1 M GdmCl, *Bs*-CspB is completely folded, and above 3 M GdmCl, it is completely unfolded (cf. Figure 4A). When pressure jumps such as those shown in Figure 2 were performed in the absence of GdmCl or in the presence of 3.3 M GdmCl, the observed fluorescence remained constant (Figure 3). These control experiments suggest that processes other than unfolding and refolding do not contribute to the fluorescence changes observed (as in Figure 2) following the pressure jumps.

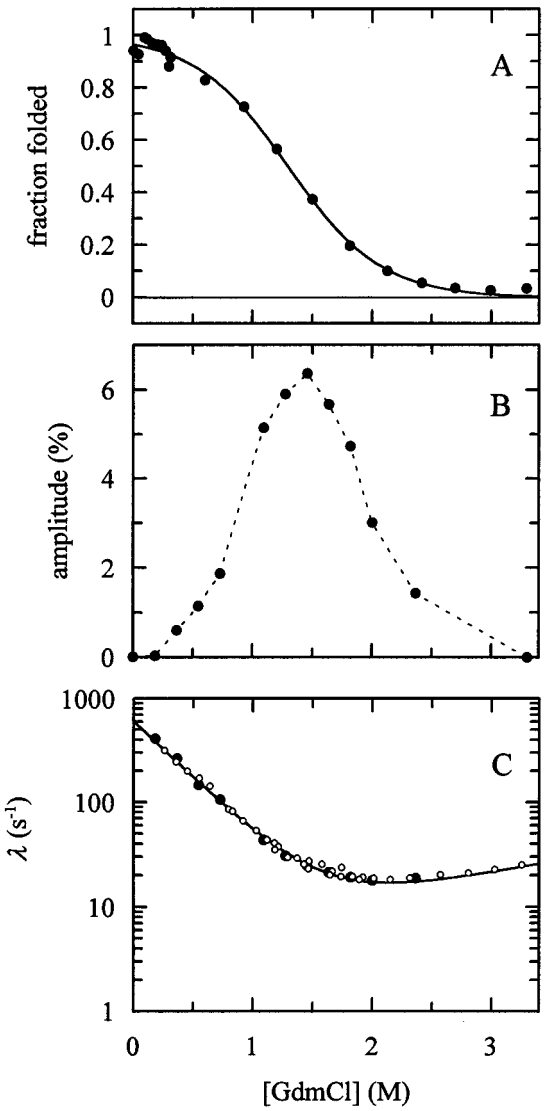

FIGURE 4: (A) Guanidinium chloride-induced equilibrium unfolding transition curve of CspB. (B) Amplitudes and (C) apparent rate constants of refolding (●) as a function of GdmCl concentration. Refolding kinetics of 12 μM wild-type CspB were followed by fluorescence after a pressure jump from 160 to 3 bar. The reaction amplitudes in panel B are shown as a percentage of the initial 10 V signal. The folding rates in panel C are compared with results from stopped-flow experiments (○) under the same conditions. These data and the line were taken from ref *36*. All experiments were performed in 0.1 M sodium cacodylate/HCl at pH 7.0 and 25 °C. The line in panel A represents the analysis based on a linear two-state model (*39*).

In further pressure-induced folding experiments as shown in Figure 2, the GdmCl concentration was varied between 0.3 and 2.4 M. The observed amplitudes and rate constants (λ) are shown in panels B and C of Figure 4, respectively, together with the equilibrium unfolding transition (in panel A). The shift of the U ⇌ N equilibrium with a 160 bar pressure jump should be maximal at the midpoint of the transition. This is indeed observed. The amplitudes of refolding show a bell-shaped dependence on denaturant concentration (Figure 4B) with a maximum near 1.5 M GdmCl.

In Figure 4C, the apparent rate constants of refolding (λ) from the 160 to 3 bar pressure-jump experiments are compared with the previously published rate constants of folding derived from stopped-flow experiments under the

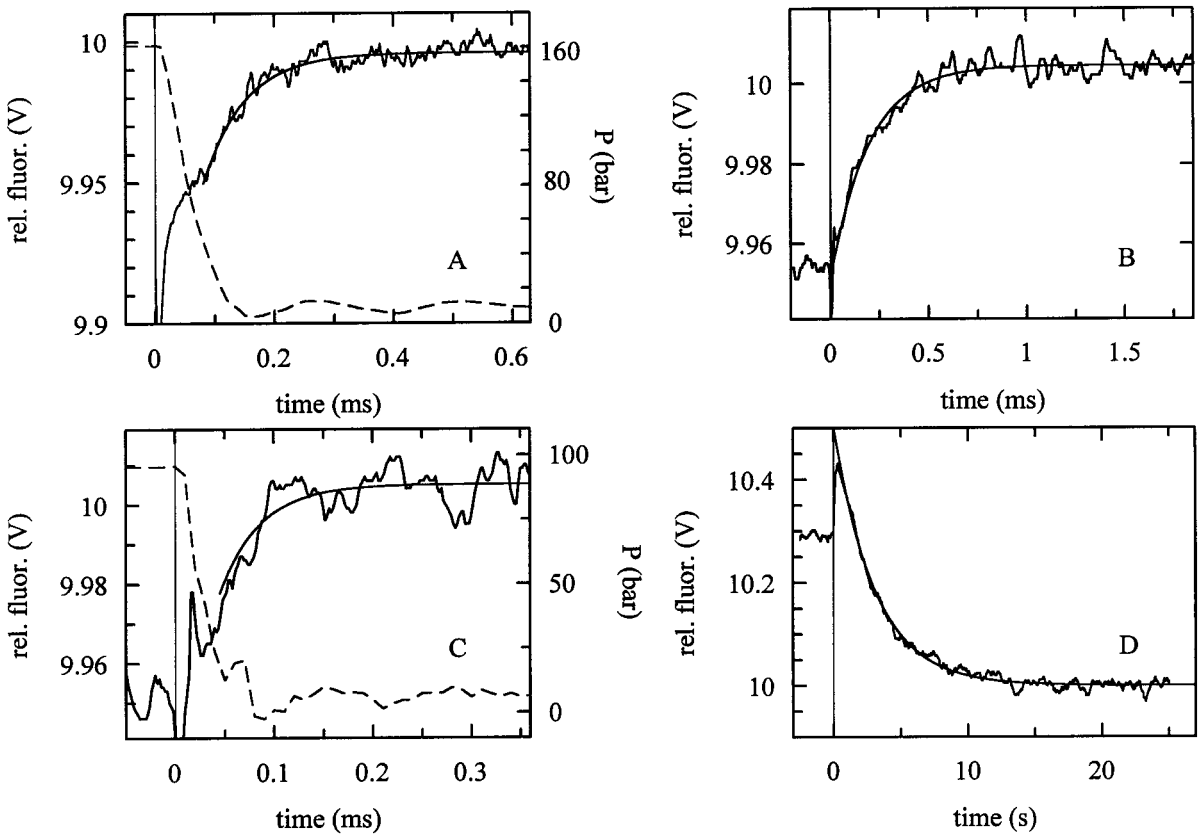

FIGURE 5: Representative folding kinetics after pressure jumps. (A) Refolding of 10 μM *Bs*-CspB(F27A) following a pressure jump from 160 to 3 bar at 65.1 °C. (B) Refolding of 6 μM *Bc*-Csp after a pressure jump from 100 to 3 bar at 75.3 °C. (C) Refolding of 6 μM *Bc*-Csp following a pressure jump from 100 to 3 bar at 79.7 °C. (D) Refolding of 3 μM *Bs*-CspB following a pressure jump from 160 to 1 bar in 95% (grams per 100 mL) ethylene glycol at 35 °C. All experiments were performed in 0.1 M sodium cacodylate/HCl at pH 7.0. The kinetics depicted in panels A and B were measured 200 times and those depicted in panel C 300 times and averaged. The kinetics depicted in panel D represent a single experiment. The solid lines represent best fits to monoexponential time courses. The respective time constants are (A) 70 μs, (B) 197 μs, (C) 41 μs, and (D) 3.1 s (slow phase). The dashed lines in panels A and C give the pressure profiles (right ordinates).

same conditions (*36*). The coincidence between the two data sets is remarkably good and indicates that both techniques are free of systematic errors.

Time Range of Pressure-Jump-Induced Folding. Depending on the choice of the piezo element, the final pressure is reached within 50−100 μs of the initiation of the jump and then kept constant in the reaction cell. We found that the long-term stability of the final pressure was good enough to collect folding data between 70 μs and 70 s; i.e., the accessible time range spans at least 6 orders of magnitude. Representative folding kinetics are shown in Figure 5. Figure 5A shows refolding kinetics of the Phe27Ala form of *Bs*-CspB at 65 °C. This variant is less stable and unfolds much more rapidly than wild-type *Bs*-CspB. At 65 °C, the N ⇌ U unfolding transition is about 95% complete (cf. Figure 5A). Therefore, the increase in the fraction of N molecules after the 160 to 3 bar pressure jump is small, and the measured rate constant is largely determined by the microscopic rate constant of unfolding. The amplitude of refolding after the 160 to 3 bar pressure jump in Figure 5A is only about 0.3% of the final fluorescence value. The kinetics of folding were, however, obtained with a good signal/noise ratio after averaging the results of 200 repetitive pressure cycles, which were performed within 20 s. The N ⇌ U equilibration reaction of Phe27Ala-*Bs*-CspB is very rapid and exhibits a time constant of 70 μs. The pressure profile in Figure 5A shows that 90% of the final pressure is reached within 100 μs.

Figure 5B shows the refolding kinetics of *Bc*-Csp obtained after a 100 to 3 bar pressure jump near the upper end of the thermal unfolding transition of this molecule (at 75 °C) and in the absence of GdmCl. *Bc*-Csp is more stable than *Bs*-CspB, and therefore, its unfolding and refolding can be followed at high temperatures. A smaller piezoelectric element was used in these experiments, because the pressure changes are established more rapidly (90% complete within about 50 μs; cf. the pressure profile in Figure 5C) with this element. The estimated rate constant λ for folding of *Bc*-Csp at 75 °C is 5000 ± 400 s^{-1}, and the amplitude is 0.5% of the final value (Figure 5B).

The measured rate constant λ is the sum of the microscopic rate constants of unfolding and refolding, k_{NU} and k_{UN}, respectively (eq 4b). The equilibrium constant K_{NU} ($=k_{NU}/k_{UN}$) is known from the thermally induced equilibrium unfolding transition, and thus, the individual values of k_{NU} and k_{UN} can be calculated from λ and K_{NU}. At 75 °C, values of microscopic rate constants for unfolding and refolding, k_{NU} and k_{UN}, of 3700 and 1400 s^{-1}, respectively, could be derived for *Bc*-Csp.

A refolding trace observed for *Bc*-Csp after a 100 to 3 bar pressure jump at 80 °C is shown in Figure 5C. At this temperature, folding is so fast that the increase in protein

fluorescence almost follows the pressure profile. The comparison of the pressure profiles and the folding kinetics indicates that the fluorescence data at times greater than 50 μs can be used for the analysis of the folding kinetics. From these data, a time constant of about 40 μs can be estimated for folding at this temperature. This experiment marks the limit of resolution of the pressure-jump experiments and suggests that folding reactions with rate constants of >10000 s^{-1} and amplitudes smaller than 1% can be investigated. It should be noted that the 300 pressure jump cycles of the experiment whose results are depicted in Figure 5C were collected within only 30 s.

The rapid folding of *Bs*-CspB is strongly retarded in the presence of viscosogenic additives such as ethylene glycol (*38*). The very slow folding of *Bs*-CspB in 95% ethylene glycol ($\eta_{rel} = 11$) was used to test the suitability of the pressure-jump cell for following very slow folding reactions in highly viscous solvents. The kinetics observed after a 160 to 5 bar pressure jump occur in the range of 30 s (Figure 5D). The fluorescence signal is stable within this time range, which shows that the pressure-jump apparatus can be used to follow folding reactions with small amplitudes in the microsecond to minute time range. Intriguingly, an increase followed by a decrease in fluorescence is observed for refolding (Figure 5D), an observation that merits further investigation. Pressure-jump methods are ideally suited to studying relaxation processes in highly viscous solvents because a fast flow and mixing of solutions is not required to initiate the reaction.

Activated State of Folding of Bs-CspB. The folding reactions of the cold shock proteins are very fast; they follow a simple, reversible U $\rightleftharpoons$ N two-state mechanism, and the activated state of folding is unusually native-like (*6*, *7*, *36*, *38*). Here we used the pressure-jump technique to determine the thermodynamic activation parameters $\Delta G^{\ddagger}$, $\Delta H^{\ddagger}$, $\Delta C_p^{\ddagger}$, and $\Delta S^{\ddagger}$ of the folding reactions of wild-type *Bs*-CspB and of the Phe15Ala, Phe17Ala, and Phe27Ala variants. These partially exposed Phe residues are located in β-strands 2 and 3 (*43*) and are important for the stability of the folded protein (*37*). Here we asked whether these Phe residues are also important for the kinetics of folding and how they contribute to the energetics of the activated state of folding.

The pressure-jump method is very well suited to determining the thermodynamic activation parameters of a reversible folding reaction from its dependence on temperature. Measurements can be performed between 5 and 80 °C; a single sample can be used for all measurements, and the reversibility is routinely examined by comparing the unfolding and refolding kinetics in the course of the pressure up and down cycles. In our previous work, the $\Delta H^{\ddagger}$ and $\Delta C_p^{\ddagger}$ values for unfolding and refolding of wild-type *Bs*-CspB were obtained with a laborious procedure in which the unfolding and refolding kinetics were first measured as a function of urea concentration at 14 different temperatures and then extrapolated to 0 M urea (*6*). This procedure was confined to temperatures of $\leq$50 °C; it consisted of several thousand individual stopped-flow experiments and required about 20 mg of protein. With the pressure-jump method, the temperature dependence of the folding kinetics of a particular protein could be determined with a single 0.2 mL sample, which contained less than 20 μg of protein. An extrapolation to denaturant-free conditions was not necessary; the measurements were, however, confined to the transition region.

The dependencies on temperature of the microscopic rate constants of unfolding and refolding, k_{NU} and k_{UN}, are determined by the activation parameters $\Delta H^{\ddagger}$ and $\Delta C_p^{\ddagger}$ (eqs 5 and 6). In principle, the microscopic rate constants at a reference temperature and the activation parameters could be derived from an analysis of the λ values based on a combination of eqs 4−6. To avoid such a six-parameter fit with a limited set of data, we made use of the two-state character of the folding transition of *Bs*-CspB (*6*, *7*) and calculated the microscopic rate constants as a function of temperature by combining the equilibrium ($K = k_{NU}/k_{UN}$) and kinetic ($\lambda = k_{NU} + k_{UN}$) data.

The thermal unfolding transitions of wild-type *Bs*-CspB and the three Phe → Ala variants were measured by the decrease in circular dichroism at 223 nm (Figure 6A). The Phe → Ala mutations are so strongly destabilizing (*37*) that for the mutated proteins the baselines for the native forms are not reached at low temperatures. These baselines were therefore measured separately in the presence of 36% ethylene glycol, which strongly stabilizes *Bs*-CspB and its variants (*38*) but does not affect the circular dichroism of native *Bs*-CspB at 223 nm and its dependence on temperature. The thermodynamic parameters obtained from the analysis of the transitions in Figure 6A are shown in Table 1, and they are independent of the protein concentration. Alternative analyses without fixed baselines for the native proteins gave overall similar results. There were, however, large uncertainties in the values obtained for ΔC_p, which depend strongly on the baselines of a transition.

The folding kinetics could be measured by the pressure-jump technique over a wide range of temperatures because the thermal transitions are broad (cf. Figure 6A). For the Phe27Ala variant, the transition extends from 10 to 65 °C. As outlined above, the microscopic rate constants of unfolding and refolding, k_{NU} and k_{UN}, were calculated from λ and K. The Arrhenius plots in panels B and C of Figure 6 show k_{UN} and k_{NU} as a function of temperature. For all four forms of *Bs*-CspB, the plots for unfolding (Figure 6C) are almost linear, whereas those for refolding in Figure 6B are strongly curved, indicating that the $\Delta C_p^{\ddagger}$ of unfolding is virtually zero.

The thermodynamic activation parameters $\Delta G^{\ddagger}$, $\Delta H^{\ddagger}$, $\Delta C_p^{\ddagger}$, and $\Delta S^{\ddagger}$ of unfolding and refolding at 45 °C for wild type *Bs*-CspB and the three Phe → Ala variants are given in Table 1. At this temperature, the equilibrium constants of folding of all proteins could be determined directly from the thermal transitions (Figure 6A), and therefore, the propagation of errors from the equilibrium to the activation parameters was minimal under these conditions. The activation enthalpies of unfolding are high for all four proteins and vary between 120 and 140 kJ/mol. The activation enthalpies of refolding are all negative because $\Delta C_p^{\ddagger}$ of refolding exhibits a large negative value. They range from −17 to −44 kJ/mol. The variations in the $\Delta H^{\ddagger}$ values are much larger than those in $\Delta G^{\ddagger}$. This is most clearly seen in the refolding of the Phe15Ala variant. The enthalpic barrier of its refolding ($\Delta\Delta H^{\ddagger}$) is reduced by about 20 kJ/mol, but the entropic barrier ($\Delta T\Delta S^{\ddagger}$) is increased by about 25 kJ/mol (Table 1); thus, the net activation free energy is increased by only 5 kJ/mol.

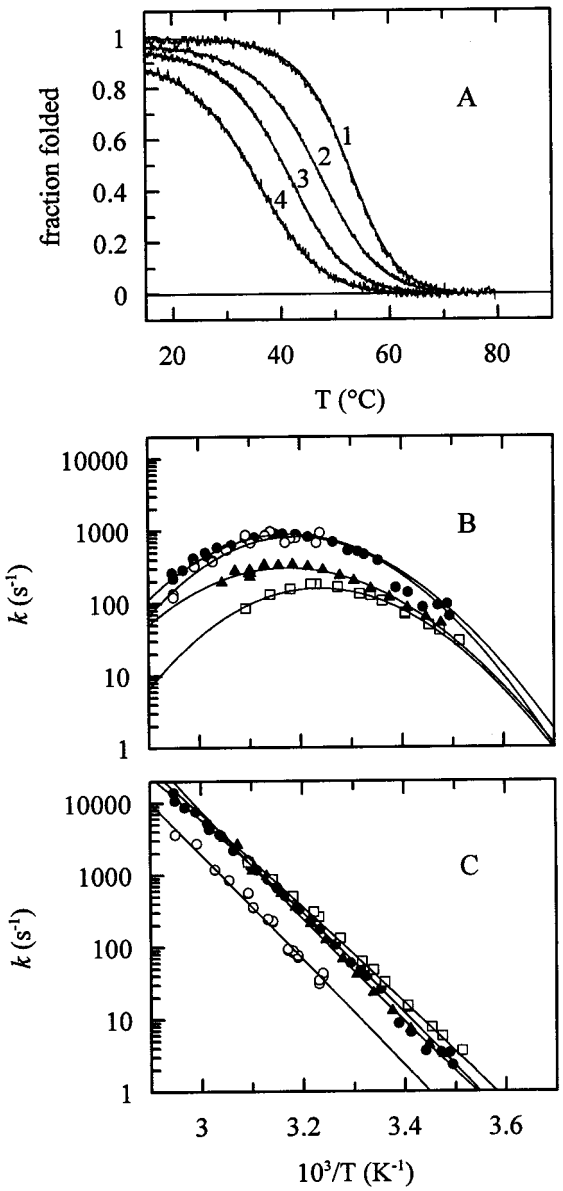

FIGURE 6: (A) Heat-induced equilibrium unfolding transitions of wild-type *Bs*-CspB (curve 1) and the Phe27Ala (curve 2), Phe17Ala (curve 3), and Phe15Ala (curve 4) variants. The transitions were monitored by the increase in circular dichroism at 223 nm. The protein concentrations were 3 μM. The unfolding curves were analyzed on the basis of a two-state mechanism as described in Materials and Methods. The fractions of folded protein are plotted as a function of temperature. The results of the analysis (continuous lines) are given in Table 1. (B) Arrhenius plot of the microscopic rate constant k_{UN} of refolding of (○) wild-type *Bs*-CspB and the (●) Phe27Ala, (▲) Phe17Ala, and (□) Phe15Ala variants. (C) Arrhenius plot of the microscopic rate constant k_{NU} of unfolding of (○) wild-type *Bs*-CspB and the (●) Phe27Ala, (▲) Phe17Ala, and (□) Phe15Ala variants. The protein concentration was 10 μM in 0.1 M sodium cacodylate/HCl at pH 7.0. The kinetics were measured 4−300 times and averaged. The solid lines in panels B and C represent the results of the analyses based on eqs 3−6 (see Materials and Methods). The resulting activation parameters are given in Table 1.

Table 1: Thermodynamic Parameters for Equilibrium Unfolding (N ⇌ U) and Activation Parameters for Refolding (U → TS) and Unfolding (N → TS) of Wild-Type *Bs*-CspB and Variants F27A, F17A, and F15A at 45 °C[a]

N ⇌ U	ΔG (kJ/mol)	ΔH (kJ/mol)	ΔS (J mol^{-1} K^{-1})	ΔC_p (kJ mol^{-1} K^{-1})
wild-type	4.89 ± 0.04	161 ± 2	493 ± 5	4.7 ± 0.6
F27A	1.16 ± 0.04	140 ± 2	439 ± 5	3.8 ± 0.5
F17A	−1.46 ± 0.04	153 ± 3	488 ± 9	4.1 ± 0.3
F15A	−3.67 ± 0.04	157 ± 8	510 ± 26	3.9 ± 0.5
U → TS	$\Delta G^{\ddagger}$ (kJ/mol)	$\Delta H^{\ddagger}$ (kJ/mol)	$\Delta S^{\ddagger}$ (J mol^{-1} K^{-1})	$\Delta C_p^{\ddagger}$ (kJ mol^{-1} K^{-1})
wild-type	60.6 ± 0.5	−24 ± 8	−266 ± 24	−4.8 ± 0.9
F27A	60.1 ± 0.5	−16.9 ± 1.0	−242 ± 5	−4.2 ± 0.4
F17A	62.9 ± 0.3	−14.3 ± 3.3	−243 ± 11	−3.8 ± 0.6
F15A	65.3 ± 0.2	−44.4 ± 9.2	−345 ± 30	−4.6 ± 0.6
N → TS	$\Delta G^{\ddagger}$ (kJ/mol)	$\Delta H^{\ddagger}$ (kJ/mol)	$\Delta S^{\ddagger}$ (J mol^{-1} K^{-1})	$\Delta C_p^{\ddagger}$ (kJ mol^{-1} K^{-1})
wild-type	64.4 ± 0.5	137 ± 5	226 ± 15	−0.1 ± 0.3
F27A	60.7 ± 0.5	123 ± 2	196 ± 5	−0.5 ± 0.1
F17A	61.0 ± 0.3	139 ± 3	245 ± 9	0.4 ± 0.4
F15A	60.4 ± 0.2	122 ± 5	193 ± 14	−0.2 ± 0.3

[a] All measurements were performed in 0.1 sodium cacodylate/HCl at pH 7.0. The thermodynamic parameters were obtained from fits of equilibrium unfolding transition curves as shown in Figure 6A, and the activation parameters were obtained from fits to the kinetic data shown in panels B and C of Figure 6 by using eqs 4b,c, 5, and 6.

DISCUSSION

Pressure-Jump-Induced Protein Folding. Fast up and down pressure jumps are well suited to initiating protein unfolding and refolding reactions. With our apparatus, the pressure can be changed by 160 bar in 100 μs and by 100 bar in 50 μs. No flow of reactants is necessary, and therefore, pressure-jump kinetics are not plagued by mixing artifacts. Reactions in highly viscous solvents can be followed with ease, and the time window that is accessible in a single experiment extends from the microsecond to minute time range, i.e., more than 6 orders of magnitude. In the refolding experiments with the cold shock proteins described here, reactions with time constants between 41 μs and 3.1 s were followed. Up and down jumps in pressure can be performed with equal precision. Therefore, the reversibility of pressure-induced unfolding and refolding can be checked easily, and a single sample can be used for many repetitive measurements either under the same conditions to improve the quality of the data or as a function of temperature to obtain the thermodynamic activation parameters of a folding reaction. Pressure-jump experiments thus require only minute amounts of material.

For complete unfolding, pressures of >1000 bar are usually required. Therefore, it is not possible to perform baseline unfolding and refolding experiments with the current experimental setup, and the measurements are restricted to the transition region of a thermally or denaturant-induced folding transition. In the design of our experiments, we had to weigh the rapidity of the pressure change against the magnitude of the change in signal. By using pressure jumps between 100 and 160 bar, we could keep the apparent dead time below 100 μs and still induce changes in fluorescence that allowed measurements at protein concentrations as low as 0.02 mg/mL.

The observed folding kinetics generally became slower with increasing pressure. This was found at the onset of the thermal unfolding transitions, where the observed kinetics are dominated by refolding, as well as at the end of the transitions, where the observed kinetics are dominated by unfolding. This shows that the activation volumes of both unfolding and refolding are positive; i.e., in the activated state, the system has a higher volume than in the native and unfolded ground states. We can, however, not give explicit

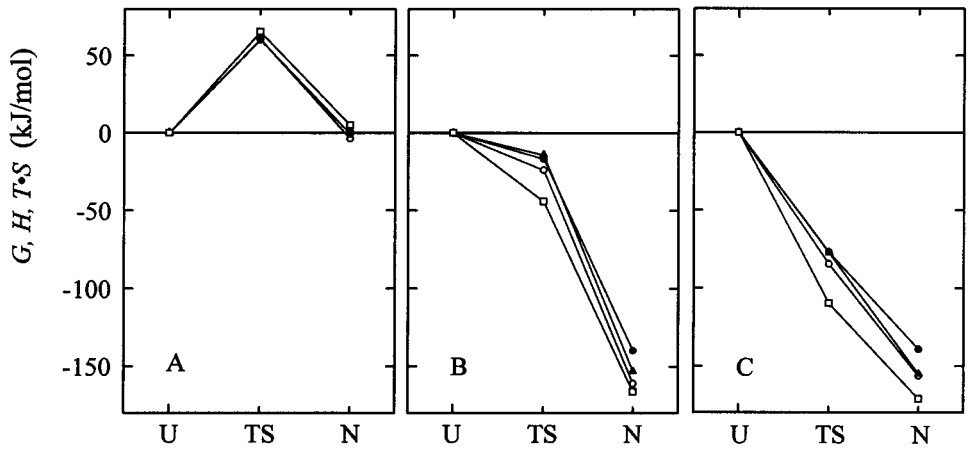

FIGURE 7: Reaction profiles for the folding of (○) wild-type *Bs*-CspB and the (●) Phe27Ala, (▲) Phe17Ala, and (□) Phe15Ala variants at pH 7.0 and 45 °C when going from the unfolded state (U) via the transition state (TS) to the native state (N): (A) Gibbs free energy *G*, (B), enthalpy *H*, and (C) entropy, expressed as *TS*. The traces are arbitrarily aligned such that the values for U coincide (and are set to zero).

numbers for the activation volumes, because they are small and because the pressure can be changed only in the range of 1−160 bar.

Comparison with Other Methods for Following Fast Folding Reactions. Our method is most closely related to the temperature-jump technique. Infrared lasers can be used to increase the temperature of a solution in several nanoseconds; therefore, the time resolution of this method is extremely high, and folding processes that occur in <1 μs can be studied (*25*, *27*). Only jumps to higher temperatures are possible, and therefore, rapid repetitive cycles of up and down jumps (as with pressure) for examining the reaction in either direction are not possible. The increased temperature after the jump is maintained only for a very short period of time, and therefore, the temperature-jump method is restricted to times shorter than 1 ms.

Two other techniques show a time resolution similar to that of the pressure-jump method. When ultrarapid turbulent mixing was combined with detection at continuous flow, the dead time of several folding reactions could be reduced to <100 μs (*8*−*10*). The advantage of this method is that the solvent conditions can be changed in the mixing step, and thus, refolding can be studied under conditions that strongly favor the native state. Careful controls are necessary in this method to account for fluctuations in the signal that are caused by the turbulent mixing. Large amounts of protein are necessary for this continuous-flow technique, and the observation time is restricted to <1 ms.

Oas and co-workers used exchange broadening of NMR signals caused by the equilibration between the native and the unfolded state of a protein to determine the dynamics of folding (*4*, *12*). This method has a time resolution of about 0.5 ms, which can be extended to about 250 μs by including T_2 relaxation data. Exchange broadening can also be applied only in the transition region where both the native and unfolded states of a protein are populated.

Optical triggering of folding reactions is restricted to proteins, which can be induced to fold by a photochemical process, such as the reduction of cytochrome *c* by a light-sensitive reductant (*21*−*23*).

Clearly, there is no single method of choice for following fast events in protein folding. Rather, the various techniques complement each other. Early events in complex folding reactions that are complete in <1 ms are best followed after turbulent mixing or after a laser-induced increase in temperature, which is possible only for a cold-unfolded protein, such as myoglobin (*25*−*27*). The pressure-jump method is ideally suited to investigating the kinetics of very fast folding proteins under a wide variety of conditions. Since folding or unfolding is initiated by the rapid change in an external variable (pressure), the other variables, such as temperature, denaturant concentration, or solvent viscosity, can be changed at will. Therefore, an almost unlimited range of folding conditions can be sampled. As shown here for the cold shock proteins, the method is particulary valuable for following the folding kinetics over a wide range of temperatures and for investigating the folding of thermostable proteins at high temperatures. The experiments can be repeated many times in an automated fashion and require only minimal amounts of proteins. The time resolution of the method can, in principle, be further improved by integrating the pressure profile (which is recorded simultaneously; cf. Figure 5) into the analysis.

Influence of the Partially Exposed Phenylalanine Residues on the Energetics of Folding of Bs-CspB. On the exposed side of its β-sheet, *Bs*-CspB contains, among others, three Phe residues at positions 15, 17, and 27. Although all three of them are only partly buried in the native state, their individual substitution by alanine is destabilizing. The Phe15Ala substitution in particular reduces the stability by more than 70% (cf. Table 1).

The comparative analysis of the folding kinetics of wild-type CspB and the three Phe → Ala variants as a function of temperature provides both global and local information about the activated state of folding. The three substitutions do not change the overall properties of the activated state relative to those of the folded state. The activated states (or, to be more precise, the ensemble of activated states) of all four forms of *Bs*-CspB exhibit the same heat capacities as the native states, and the enthalpies drop by 120−140 kJ/mol in the final phase of folding from the activated to the native states. This temperature-independent decrease in enthalpy reflects the asynchrony of the loss in chain entropy and the gain of stabilizing interactions in the folding of the cold shock protein. The activated state is reached when this asynchrony is most pronounced. The gain in stabilizing

interactions after passage through the activated state is probably distributed over the entire protein, and thus, single substitutions as in the cases described here have only small effects.

Although the three Phe → Ala mutations do not change the global properties of the activated state, they have distinct effects on the microscopic rates of folding. The Phe27Ala mutation increases only the rate of unfolding, whereas the rate of refolding and its dependence on temperature are virtually unchanged. This suggests that in the entire temperature range Phe27 is still in an unfolded-like environment in the activated state of refolding and becomes ordered only after the activated state. The Phe15Ala and Phe17Ala substitutions have mixed effects. They retard refolding and accelerate unfolding, indicating that Phe15 and Phe17 are in partially ordered environments in the activated state. Phe15Ala, which destabilizes the folded protein most strongly (by 8 kJ/mol, Table 1), also retards refolding most strongly.

Analyses of the folding kinetics as a function of temperature as depicted in Figure 6 can, in principle, be used to determine the contributions of individual residues not only to the activation free energy but also to the activation enthalpy and entropy. The data in Table 1 and the plots of *G*, *H*, and *TS* as a function of the reaction coordinate (Figure 7) indicate that the Phe → Ala mutations lead to compensatory changes in activation enthalpies and entropies. It is not yet possible to analyze this enthalpy/entropy compensation quantitatively, because of the delicate interdependence of the equilibrium and activation enthalpies and heat capacities. It should also be noted that the activation entropies (and also the activation free energies) depend on the pre-exponential factor in the Eyring equation, which is not known for protein folding reactions. Therefore, only the changes caused by mutations, but not the absolute value, can be interpreted with confidence.

In summary, our results indicate that the three Phe → Ala mutations in *Bs*-CspB do not change the overall character of the activated state of folding, which is native-like but still lacks many enthalpic interactions. The substitution of Phe27 destabilizes the folded state only to a minor extent, and at the same time ordering of this residue is not required in the activated state. The substitutions of Phe17 and, in particular, of Phe15 are more strongly destabilizing. Interactions provided by these two residues are fairly unimportant for folding at low temperatures, but become more important when the temperature is increased. The activated state thus seems to move even closer to the native state with increasing temperature, a move which is seen at the level of individual residues, but not in the gross properties of the activated state. This suggests that the activated state of folding of CspB follows Hammond-type behavior (cf. the discussion by Fersht and co-workers in ref *45*). A strong enthalpy/entropy compensation as in the equilibrium stability of folded proteins is also observed for the activated state. The large and compensatory changes in the activation enthalpies and entropies lead to small changes in the Gibbs free energy of activation and provide clear evidence for the important role of solvent interactions for the activated state of folding.

ACKNOWLEDGMENT

We thank K. Schröder and V. Sieber for strains of *E. coli* that overproduce the Phe → Ala variants of *Bs*-CspB and J. Balbach and C. Scholz for discussions. M. A. Geeves thanks R. M. Clegg and E. L. Elson for invaluable advice on the design of the pressure-jump apparatus. This work was initiated by the EMBO practical course on kinetics, Dortmund, 1997.

REFERENCES

1. Jaenicke, R. (1987) *Prog. Biophys. Mol. Biol. 49*, 117−237.
2. Jaenicke, R. (1996) *Curr. Top. Cell. Regul. 34*, 209−314.
3. Jackson, S. E., and Fersht, A. R. (1991) *Biochemistry 30*, 10428−10435.
4. Huang, G. S., and Oas, T. G. (1995) *Proc. Natl. Acad. Sci. U.S.A. 92*, 6878−6882.
5. Kragelund, B. B., Robinson, C. V., Knudsen, J., Dobson, C. M., and Poulsen, F. M. (1995) *Biochemistry 34*, 7217−7224.
6. Schindler, T., Herrler, M., Marahiel, M. A., and Schmid, F. X. (1995) *Nat. Struct. Biol. 2*, 663−673.
7. Schindler, T., and Schmid, F. X. (1996) *Biochemistry 35*, 16833−16842.
8. Chan, C. K., Hu, Y., Takahashi, S., Rousseau, D. L., Eaton, W. A., and Hofrichter, J. (1997) *Proc. Natl. Acad. Sci. U.S.A. 94*, 1779−1784.
9. Shastry, M. C. R., and Roder, H. (1998) *Nat. Struct. Biol. 5*, 385−392.
10. Shastry, M. C. R., Luck, S. D., and Roder, H. (1998) *Biophys. J. 74*, 2714−2721.
11. Burton, R. E., Huang, G. S., Daugherty, M. A., Fullbright, P. W., and Oas, T. G. (1996) *J. Mol. Biol. 263*, 311−322.
12. Burton, R. E., Huang, G. S., Daugherty, M. A., Calderone, T. L., and Oas, T. G. (1997) *Nat. Struct. Biol. 4*, 305−310.
13. Kragelund, B. B., Hojrup, P., Jensen, M. S., Schjerling, C. K., Juul, E., Knudsen, J., and Poulsen, F. M. (1996) *J. Mol. Biol. 256*, 187−200.
14. Onuchic, J. N., Wolynes, P. G., Luthey-Schulten, Z., and Socci, N. D. (1995) *Proc. Natl. Acad. Sci. U.S.A. 92*, 3626−3630.
15. Dill, K. A., and Chan, H. S. (1996) *Nat. Struct. Biol. 4*, 10−19.
16. Tsong, T.-Y., Baldwin, R. L., and Elson, E. L. (1971) *Proc. Natl. Acad. Sci. U.S.A. 68*, 2712−2715.
17. Garel, J. R., and Baldwin, R. L. (1973) *Proc. Natl. Acad. Sci. U.S.A. 70*, 3347−3351.
18. Ikai, A., Fish, W. W., and Tanford, C. (1973) *J. Mol. Biol. 73*, 165−184.
19. Tanford, C., Aune, K. C., and Ikai, A. (1973) *J. Mol. Biol. 73*, 185−197.
20. Eaton, W. A., Thompson, P. A., Chan, C. K., Hagen, S. J., and Hofrichter, J. (1996) *Structure 4*, 1133−1139.
21. Chan, C.-K., Hofrichter, J., and Eaton, W. A. (1996) *Science 274*, 628−629.
22. Hagen, S. J., Hofrichter, J., Szabo, A., and Eaton, W. A. (1996) *Proc. Natl. Acad. Sci. U.S.A. 93*, 11615−11617.
23. Pascher, T., Chesick, J. P., Winkler, J. R., and Gray, H. B. (1996) *Science 271*, 1558−1560.
24. Nölting, B., Golbik, R., and Fersht, A. R. (1995) *Proc. Natl. Acad. Sci. U.S.A. 92*, 10668−10672.
25. Williams, S., Causgrove, T. P., Gilmanshin, R., Fang, K. S., Callender, R. H., Woodruff, W. H., and Dyer, R. B. (1996) *Biochemistry 35*, 691−697.
26. Ballew, R. M., Sabelko, J., and Gruebele, M. (1996) *Proc. Natl. Acad. Sci. U.S.A. 93*, 5759−5764.
27. Ballew, R. M., Sabelko, J., and Gruebele, M. (1996) *Nat. Struct. Biol. 3*, 923−926.
28. Michels, P. C., Hei, D., and Clark, D. S. (1996) *Adv. Protein Chem. 48*, 341−376.
29. Frye, K. J., Perman, C. S., and Royer, C. A. (1996) *Biochemistry 35*, 10234−10239.
30. Jaenicke, R. (1981) *Naturwissenschaften 70*, 332−341.
31. Brandts, J. F., Oliveira, R. J., and Westort, C. (1970) *Biochemistry 9*, 1038−1047.
32. Gross, M., and Jaenicke, R. (1994) *Eur. J. Biochem. 221*, 617−630.
33. Mozhaev, V. V., Heremans, K., Frank, J., Masson, P., and Balny, C. (1996) *Proteins 24*, 81−91.

34. Pryse, K. M., Bruckman, T. G., Maxfield, B. W., and Elson, E. L. (1992) *Biochemistry 31*, 5127−5136.
35. Schindelin, H., Herrler, M., Willimsky, G., Marahiel, M. A., and Heinemann, U. (1992) *Proteins: Struct., Funct., Genet. 14*, 120−124.
36. Schröder, K., Graumann, P., Schnuchel, A., Holak, T. A., and Marahiel, M. A. (1995) *Mol. Microbiol. 16*, 699−708.
37. Schindler, T., Perl, D., Graumann, P., Sieber, V., Marahiel, M. A., and Schmid, F. X. (1997) *Proteins: Struct., Funct., Genet. 30*, 401−406.
38. Perl, D., Welker, C., Schindler, T., Schröder, K., Marahiel, M. A., Jaenicke, R., and Schmid, F. X. (1998) *Nat. Struct. Biol. 5*, 229−235.
39. Walter, S., Hubner, B., Hahn, U., and Schmid, F. X. (1995) *J. Mol. Biol. 252*, 133−143.
40. Santoro, M. M., and Bolen, D. W. (1988) *Biochemistry 27*, 8063−8068.
41. Clegg, R. M., and Maxfield, B. W. (1976) *Rev. Sci. Instrum. 47*, 1383−1392.
42. Willimsky, G., Bang, H., Fischer, G., and Marahiel, M. A. (1992) *J. Bacteriol. 174*, 6326−6335.
43. Graumann, P. L., and Marahiel, M. A. (1998) *Trends Biochem. Sci.* (in press).
44. Schindelin, H., Marahiel, M. A., and Heinemann, U. (1993) *Nature 364*, 164−168.
45. Schnuchel, A., Wiltschek, R., Czisch, M., Herrler, M., Willimsky, G., Graumann, P., Marahiel, M. A., and Holak, T. A. (1993) *Nature 364*, 169−171.
46. Jacob, M., Schindler, T., Balbach, J., and Schmid, F. X. (1997) *Proc. Natl. Acad. Sci. U.S.A. 94*, 5622−5627.
47. Fersht, A. R. (1993) *FEBS Lett. 325*, 5−16.
48. Matouschek, A., Otzen, D. E., Itzhaki, L. S., Jackson, S. E., and Fersht, A. R. (1995) *Biochemistry 34*, 13656−13662.

BI982487I